Journal of
Medicinal Chemistry

Article

Discovery of Novel Allosteric Inhibitors of Deoxyhypusine Synthase

Yuta Tanaka, Osamu Kurasawa, Akihiro Yokota, Michael G. Klein, Koji Ono, Bunnai Saito, Shigemitsu Matsumoto, Masanori Okaniwa, Geza Ambrus-Aikelin, Daisuke Morishita, Satoshi Kitazawa, Noriko Uchiyama, Kazumasa Ogawa, Hiromichi Kimura, and Shinichi Imamura

J. Med. Chem., **Just Accepted Manuscript** • DOI: 10.1021/acs.jmedchem.9b01979 • Publication Date (Web): 06 Mar 2020

Just Accepted

is published by the American Chemical Society. 1155 Sixteenth Street N.W., Washington, DC 20036

Discovery of Novel Allosteric Inhibitors of Deoxyhypusine Synthase

Yuta Tanaka,[*,†] *Osamu Kurasawa,*[†] *Akihiro Yokota,*[†] *Michael G. Klein,*[‡] *Koji Ono,*[†] *Bunnai Saito,*[†] *Shigemitsu Matsumoto,*[†] *Masanori Okaniwa,*[†] *Geza Ambrus-Aikelin,*[‡] *Daisuke Morishita,*[†] *Satoshi Kitazawa,*[†] *Noriko Uchiyama,*[†] *Kazumasa Ogawa,*[†] *Hiromichi Kimura,*[†] *and Shinichi Imamura*[†]

[†]Pharmaceutical Research Division, Takeda Pharmaceutical Company Limited: 26-1, Muraoka-Higashi 2-chome, Fujisawa, Kanagawa 251-8555, Japan

[‡]Department of Structural Biology, Takeda California, 10410 Science Center Drive, San Diego, California 92121, United States

PDB ID codes: **1** with DHPS: 6P4V, **11g** with DHPS: 6PGR

ABSTRACT: Deoxyhypusine synthase (DHPS) utilizes spermidine and NAD as cofactors to incorporate a hypusine modification into the eukaryotic translation initiation factor 5A (eIF5A). Hypusine is essential for eIF5A activation, which, in turn, plays a key role in regulating protein translation of selected mRNA that are associated with the synthesis of oncoproteins, thereby enhancing tumor cell proliferation. Therefore, inhibition of DHPS is a promising therapeutic option for the treatment of cancer. To discover novel lead compounds that target DHPS, we conducted synthetic studies with a hit obtained via high-throughput screening. Optimization of the ring structures of the amide compound (**2**) led to bromobenzothiophene (**11g**) with potent inhibitory activity against DHPS. X-ray crystallographic analysis of **11g** complexed with DHPS revealed a dramatic conformational change in DHPS, which suggests the presence of a novel allosteric site. These findings provide the basis for the development of novel therapy distinct from spermidine mimetic inhibitors.

INTRODUCTION

Eukaryotic translation initiation factor 5A (eIF5A) is an essential protein for cell growth and survival as it plays a role in the elongation process of protein translation. During this process, eIF5A is modified to contain the unique polyamine-derived amino acid, hypusine [*N*$^{\varepsilon}$-(4-amino-2-hydroxybutyl)lysine].[1–4] Hypusine is post-translationally introduced into the ε-amino group of one specific lysine residue of eIF5A by two enzymatic reactions (Figure 1).[5,6] Deoxyhypusine synthase (DHPS) catalyzes the first reaction by cleaving the polyamine spermidine and transferring its 4-aminobutyl moiety to the lysine residue of the eIF5A precursor to form a deoxyhypusine intermediate.[7] In the second reaction, deoxyhypusine hydroxylase (DOHH) converts the deoxyhypusine-containing intermediate to the hypusine-containing mature eIF5A. This hypusination of eIF5A is critical not only for the proliferation of eukaryotic cells, but also for the regulation of protein translation of selected mRNA that are associated with the synthesis of oncoproteins, and thus enhances the proliferation of tumor cells.[4,8] In addition, a recent publication has reported that eIF5A is involved in cellular respiration

and macrophage function by regulating mitochondrial proteins, which can be linked to cancer cell metabolism.[9] Therefore, blocking the biological activity of eIF5A by inhibiting the DHPS-mediated hypusine modification of the eIF5A precursor protein may be a useful strategy that can be employed in the treatment of tumorigenic diseases.

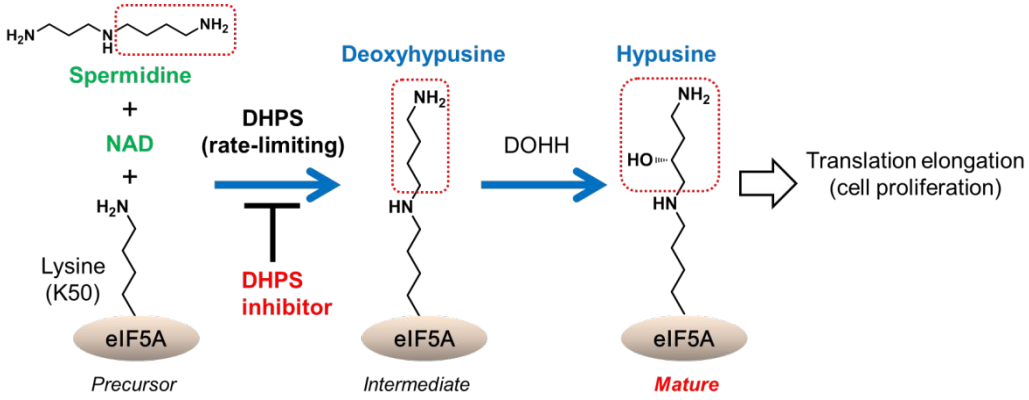

Figure 1. DHPS-eIF5A pathway as a therapeutic target for cancer.

Polyamine analogues of the natural DHPS substrate spermidine have been explored to examine their effect on DHPS activity, which led to the discovery of *N*-1-guanyl-1,7-diaminoheptane (**1**) (GC-7) as a potent DHPS inhibitor (Figure 2A).[10] Some other spermidine mimetic inhibitors were also reported as well as utilization of in silico approach to design DHPS inhibitors.[11–14] Co-crystal structure of **1** with DHPS

determined that **1** binds to the spermidine binding site.[16,17] However, the applications of **1** as a tool molecule to investigate the biology of DHPS are limited, due to its nonselective binding properties and high structural similarity to spermidine. This may cause undesired off-target pharmacology such as modulation of spermidine biosynthesis and metabolism pathways.[18,19] There is no DHPS inhibitor evaluated in clinical study because a strategy to design molecules other than spermidine mimetic inhibitors has been limited due to the lack of understanding of druggable pockets in the protein. Therefore, identification of new tool molecules possessing drug-like properties is needed to fully clarify the functions of DHPS.

(A)

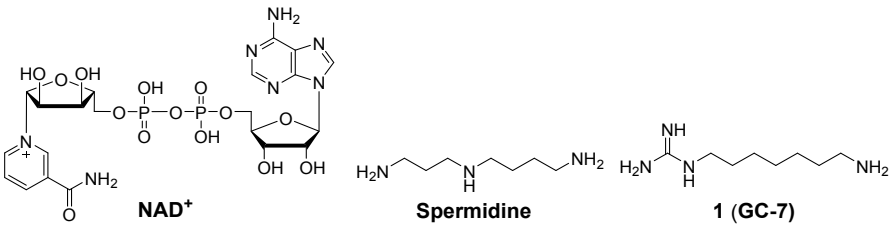

(B)

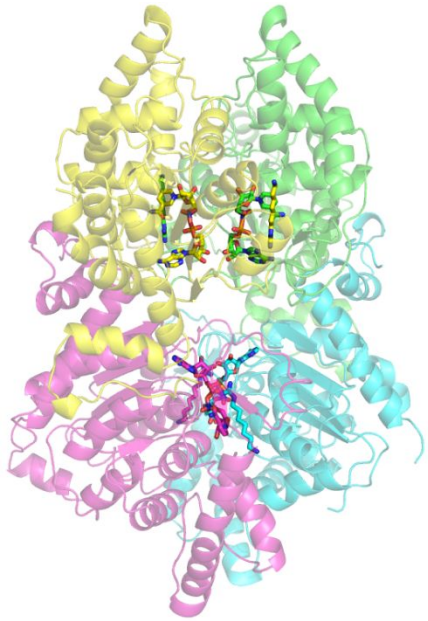

(C)

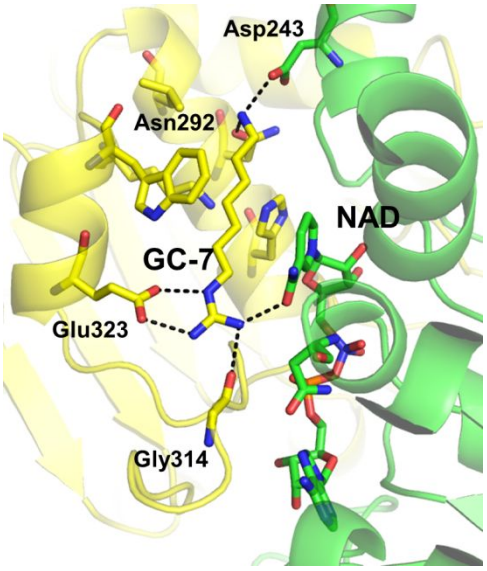

Figure 2. (A) NAD^+, spermidine, and GC-7 structures. (B) Structure of DHPS in complex with NAD and GC-7 at a resolution of 1.65 Å (PDB ID 6P4V). The protein is colored by chain and shown as a cartoon. NAD and GC-7 are shown in sticks. (C) Closeup view

highlighting the hydrogen bonds (dash lines) between GC-7 and DHPS/NAD. Residues possessing interactions with GC-7 are shown in sticks. For clarity, a part of protein is omitted. The all images were prepared using PyMOL.[15]

Here, we describe the discovery of potent DHPS inhibitors from a hit generated by a high throughput screening campaign. Furthermore, X-ray crystallographic analysis of a representative compound bromobenzothiophene **(11g)** in complex with DHPS reveals a dramatic conformational change in DHPS, suggesting the presence of a novel allosteric site. These findings open the door toward a brand-new paradigm of allosteric DHPS inhibitors with therapeutic potentials as an anti-cancer drug.

RESULTS AND DISCUSSION

X-ray Structure of DHPS with GC-7 and Profile of Hit Compound 2.

DHPS utilizes spermidine and NAD as cofactors to incorporate a 4-aminobutyl moiety onto the Lys50 side chain of eIF5A.[1,20] Initial in-house crystallography trials identified a

1.65 Å tetrameric structure of the DHPS ternary complex containing the cofactor NAD and **1** (Figure 2B, C), similar to a previously published 3.0 Å complex containing the same ligands.[17] Superposition of our 1.65 Å refined model with the published 3.0 Å structure (PDB code 1RQD) revealed a slight discrepancy in the binding pose of **1** (Supporting Information Figure S1). These data suggest that **1** is located proximal to NAD from a distinct monomer, with both ligands at the interface formed between crystallographically related DHPS molecules that pack into a larger tetrameric assembly. Hydrogens of the guanidine and amine groups of **1** interact with Glu323, Gly314, and Asn292 on one monomer and Asp243 and NAD on another monomer.

Furthermore, enzymatic inhibitory activity of **1** is not affected by the two different concentrations of NAD (14, 250 μM), suggesting that **1** and NAD molecules are not competing each other (Figure 3).[21] In contrast, compound **2**, which is a hit identified from the high throughput screening campaign, showed a NAD competitive profile; decreased potency was observed at higher concentrations of NAD. In addition, **2** exhibited a weak spermidine competitive profile (data not shown). These results

propelled studies to further optimize this molecule with the hope of discovering a novel compound distinct from spermidine mimetic inhibitors.

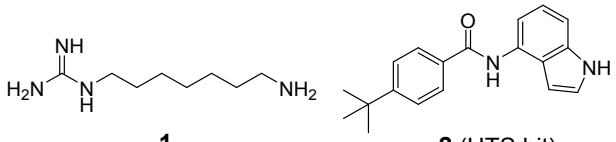

	1	**2** (HTS hit)
DHPS IC_{50} (μM)	0.14 (0.11–0.17)	0.84 (0.76–0.92)
DHPS high NAD IC_{50} (μM)	0.050 (0.043–0.055)	38 (24–61)

Figure 3. Inhibitory activity of **1** and HTS hit compound **2**. Inhibitory activity was determined by an enzyme assay in the presence of 14 or 250 μM of NAD. IC_{50} values and 95% confidence intervals (CI) were calculated by nonlinear regression analysis of percent inhibition data.

Identification of the Potent Inhibitor 11g by a Structure-Activity Relationship (SAR) study.

To identify potent inhibitors, we conducted ligand-based SAR studies, given that co-crystallization trials of **2** with DHPS failed. The inhibitory activity of derivatives possessing various linkers and scaffolds are depicted in Table 1. Conversion of the amide linker to sulfonamide (**5a**), urea (**5b**), and reverse amide (**7**) significantly

decreased potency. Regarding modification of the indole scaffold, indoline (**9a**) was not tolerated, while indolinone (**9b**) exhibited inhibitory activity (IC_{50} = 42 μM), suggesting that the acidic proton of **2** is preferable to enhance potency. In addition, orientation of the proton appears to be necessary for the function of **2** based on the IC_{50} values of pyrazole derivatives **9c** and **9d** (IC_{50} = 22 μM and >100 μM, respectively). Overall, the amide linker and indole scaffold derived from compound **2** were the best right-hand parts used for further optimization.

Table 1. SAR for Linkers and Scaffolds **2**, **5a–b**, **7**, and **9a–d**

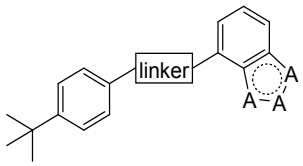

compound	linker	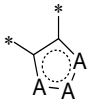	DHPS IC_{50} (μM)[a]
2 **(HTS hit)**	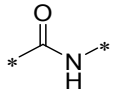	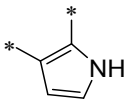	0.84 (0.76–0.92)

5a	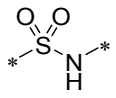	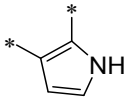	>100
5b	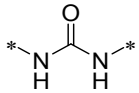	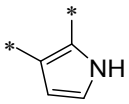	>100
7	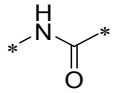	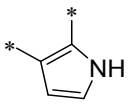	99 (68–144)
9a	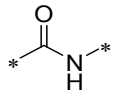	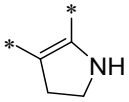	>100
9b	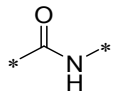	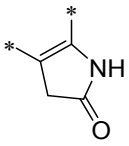	42 (30–59)
9c	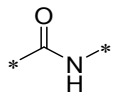	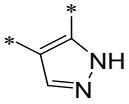	22 (9.8–50)
9d	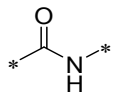	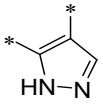	>100

[a] Determined by enzyme assay. IC_{50} values and 95% confidence intervals (CI) were calculated by nonlinear regression analysis of percent inhibition data.

Next, we attempted to convert the left-hand side of the molecule (Table 2), while maintaining the 4-aminocarbornyl indole moiety. Since removal of the *tert*-butyl group on the phenyl group of **2** decreased inhibitory activity (**11a**, IC_{50} >100 μM), we focused on examining three types of bicyclic substituents: 2-naphtyl group (**11b**), 2-benzofuranyl group (**11c**), and 2-benzothiophenyl group (**12a**). Among these, the benzothiophene derivative **12a** exhibited comparable potency to compound **2**. Additionally, we introduced a *tert*-butyl group to the benzothiophene ring to enhance the inhibitory activity in a similar fashion as **2** from **11a**, and confirmed that substitution at the 6'-position of the ring is tolerable. Although carboxamide derivative **12b** showed decreased potency, exploration of other substituents at this position (**11e–g** and **12c**) revealed that halogen substituents significantly improve DHPS inhibition. The most potent compound, 6'-bromo derivative **11g**, had an IC_{50} value of 0.062 μM. Conversely, introduction of a bromo group at the 5'- (**11h**) or 7'-position (**11i**) was unfavorable, indicating that the 6'-bromo substituent of **11g** is necessary for its binding to DHPS.

Through the SAR studies, we discovered a potent non-spermidine mimetic DHPS inhibitor **11g**.

Table 2. SAR for Left Hand Site **11a–i** and **12a–c**

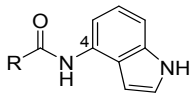

compound	R	DHPS IC_{50} (μM)[a]
2 **(HTS hit)**	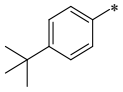	0.84 (0.76–0.92)
11a	phenyl	>100
11b	2-naphthyl	>100
11c	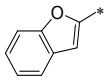	>100
12a	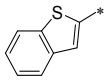	2.3 (1.5–3.6)
11d	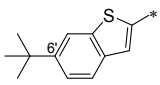	5.4

		(2.0–15)
11e	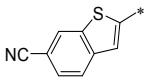	0.43 (0.24–0.77)
12b	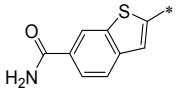	11 (5.8–20)
11f	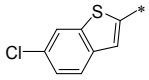	0.12 (0.093–0.17)
11g	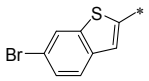	0.062 (0.045–0.084)
12c	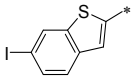	0.092 (0.069–0.12)
11h	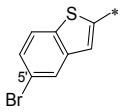	>100
11i	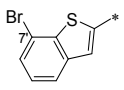	>100

[a]Refer to Table 1.

X-ray Co-crystal Structural Analysis of DHPS with 11g.

To determine the binding mode of the newly synthesized inhibitors, we solved the X-ray co-crystal structure of compound **11g** with DHPS protein at 1.95 Å resolution, as shown in Figure 4. From the results of structural analysis, a tetramer of the binary complex was identified similar to the structure of the ternary complex of **1** and NAD (Figure 4A), and **11g** was bound to a novel allosteric pocket (*vide infra*). This cocrystal structure well explained the results from the SAR studies (Figure 4B, C). Regarding the indole moiety, NH-π interaction between a side chain of His288 and the indole ring, and a hydrogen bond between Asn267 and NH of the indole were identified, confirming that it is required for potency. The amide moiety of **11g** formed a hydrogen bond network, (i) between its carbonyl oxygen and the residue Lys329 which receives the butylamine moiety of spermidine in the enzymatic reaction,[22] and (ii) between NH proton on the amide and Asp238 via a water molecule. As mentioned above, the 6-bromobenzothiophene moiety is important for enhancing inhibitory activity. It is

suggested that the fused ring needs to be positioned at an angle suitable for binding to the protein and does so by forming an intramolecular S-O interaction.[23] In addition, a unique halogen bonding between the 6-bromo group and the main chain carbonyl oxygen of Leu281 was confirmed. This interaction occurs because the extension on the Br side of the C-Br bond has a slightly positive charge.[24] Although the bromo group as a whole is a negatively charged moiety, only the site of the Br atom has the role of a "donor of hydrogen bond," enabling the interaction with the carbonyl oxygen.[25] The data of the chlorine (**11f**) and iodine (**12c**) derivatives (IC_{50} = 0.12 μM and 0.092 μM, respectively, Table 2) also support the presence of an effect as a result of halogen bonding.

(A)

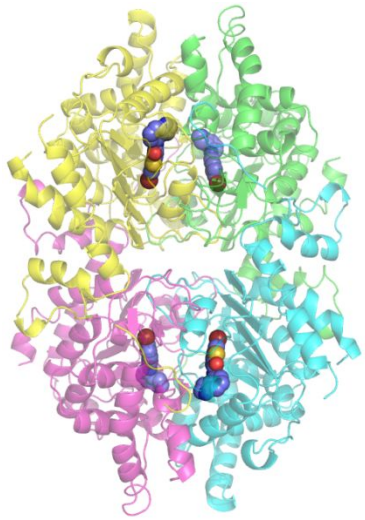

(B)

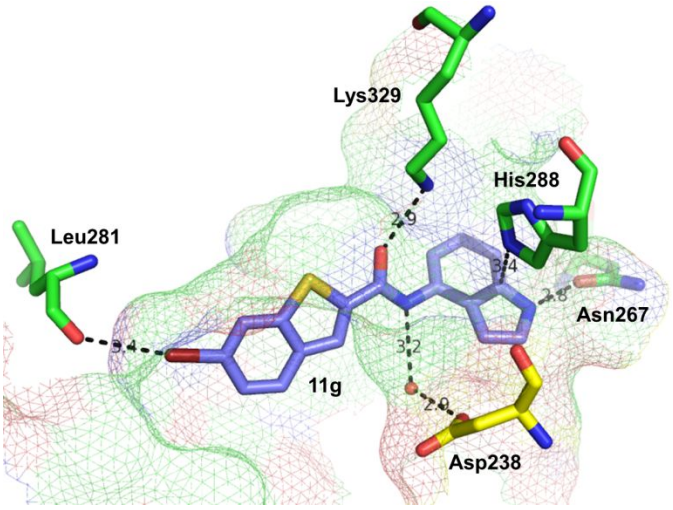

(C)

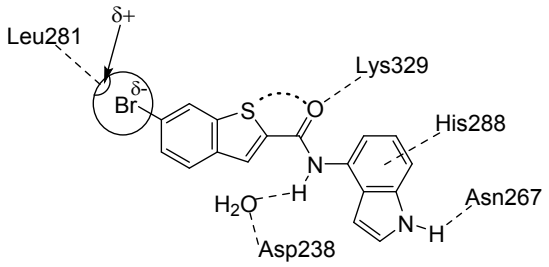

11g

DHPS IC_{50} (μM)	0.062 (0.045–0.084)
DHPS IC_{50} at high NAD (μM)	56 (9.7–325)
DHPS IC_{50} at high spermidine (μM)	6.9 (2.8–17)

Figure 4. Co-crystal structure of compound **11g** with DHPS (PDB ID 6PGR). (A) Tetramer of the structure, with each monomer indicated by a different color. **11g** is shown as spheres. (B) The allosteric binding site of **11g**. DHPS is shown at the surface. **11g** and a part of the surrounding residues are shown in sticks. The colors are the same as in (A). **11g** has hydrogen bonding interactions with Asn267, Lys329, and, moreover, with Asp238 via a crystal water molecule, shown as dash lines with the distances. **11g** also has an important interaction with His288 in NH–π interaction. For reference, the distance between the nitrogen atom of His288 and a carbon atom of the indole ring is shown. (C) Schematic diagram of interactions in stabilizing **11g** at the allosteric site. The inhibitory activity under normal conditions was determined by enzyme assay at 14 μM of NAD and 2 μM of spermidine. NAD (250 μM) or spermidine (100 μM) were used at each

condition of higher concentration, respectively. IC_{50} values and 95% confidence intervals (CI) were calculated by nonlinear regression analysis of percent inhibition data.

Observations on Dynamic Conformational Change of DHPS

To elucidate the mechanism of inhibition, profiling of **11g** inhibitory activity in the presence of high concentrations of NAD (250 μM) and spermidine (100 μM) were performed (Figure 4C). Compound **11g** was less potent both at the higher concentrations of NAD and spermidine relative to that at normal concentrations (14 μM of NAD and 2 μM of spermidine), indicating that **11g** competitively occupies the binding sites of both NAD and spermidine.

However, **11g** binds to the allosteric pocket distinct from NAD and the spermidine binding pockets as shown in Figure 5. Comparing the structural analyses of the ternary (with **1** and NAD) and binary (with **11g**) complexes, binding of **11g** appeared to induce dynamic conformational changes in the secondary structure of the protein in the vicinity of the allosteric pocket. Strikingly, the α-helix in the co-crystal structure with **1** and NAD

is unfolded and forms a loop structure in the **11g**-bound structure. Furthermore, Gly282 on the unfolded loop partially occupies the NAD binding pocket, hindering the binding of NAD (Figure 5B). In addition, Lys287 in the α-helix in the ternary (with **1** and NAD) complex dramatically moves and overlaps the spermidine binding site, indicating an interference of the binding of spermidine by **11g** (Figure 5C). Therefore, the drastic change in the secondary structure of the protein may be accompanied by the interference of both NAD and spermidine binding pockets, and thus **11g** competed with NAD and spermidine regardless of its allosteric binding characteristics.

(A)

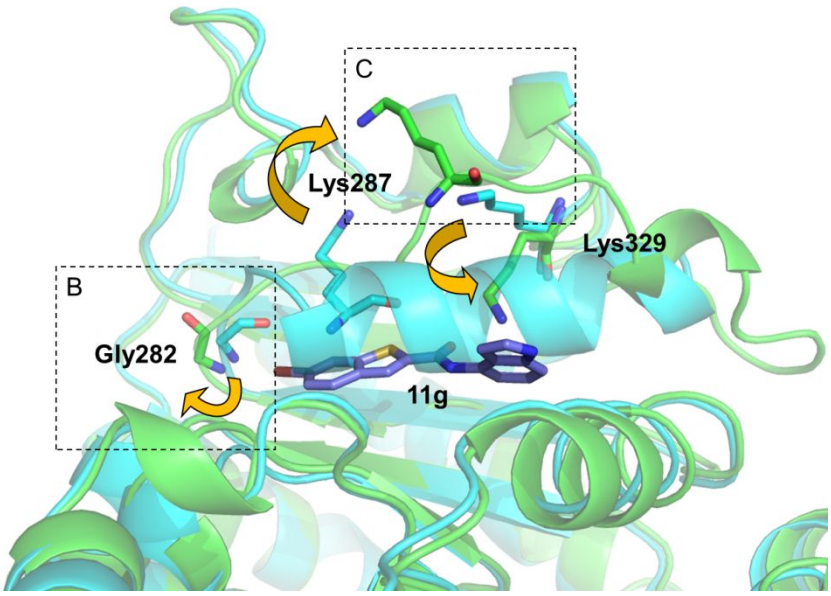

(B)

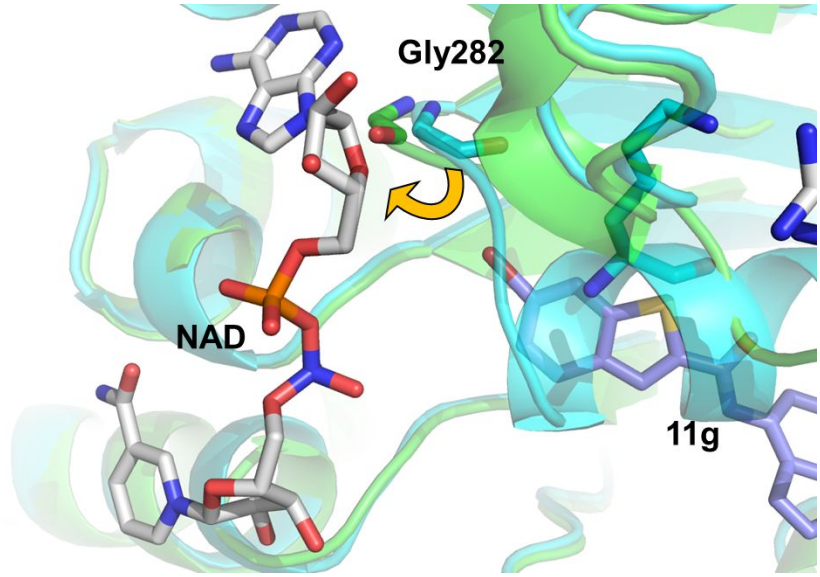

(C)

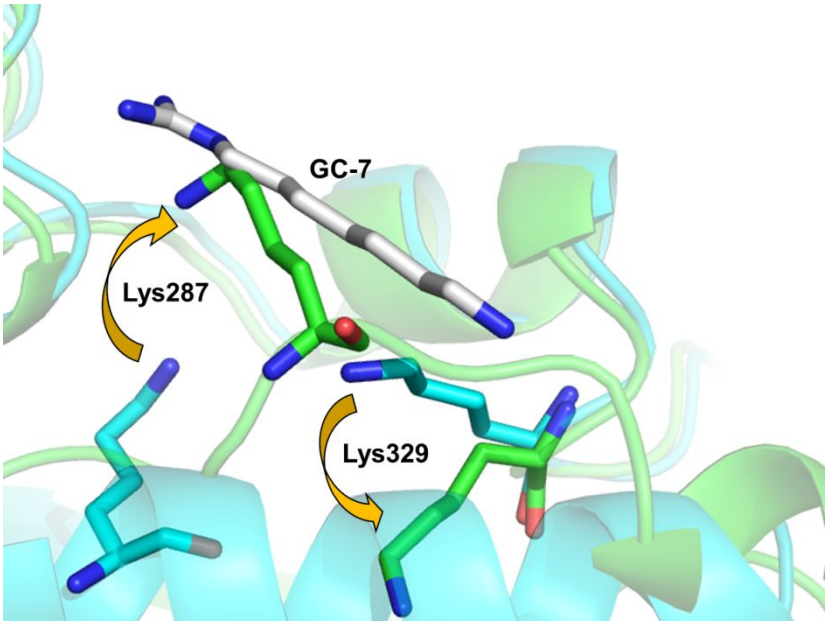

Figure 5. Superposition of the co-crystal structures of **11g**-bound and GC-7-bound forms (PDB IDs 6P4V and 6PGR). The **11g**-bound protein, the GC-7-bound protein, and

11g molecule are shown in green, cyan, and purple, respectively. (A) Comparison of the **11g**-bound and GC-7-bound forms. Ligand binding causes unfolding of an α-helix, specifically, a flip of Gly282 located near the NAD binding site and movement of Lys287 and the side chain of Lys329, which receives the butylamine moiety of spermidine in the enzymatic reaction. (B) A closeup view highlighting the NAD binding site. NAD in the GC-7 bound form is shown as a white stick. The steric clash is possible between flipped Gly282 in the **11g**-bound form and NAD in the GC-7-bound form. The closest distance between them (the oxygen atom in Gly282 and the 1' carbon in adenosine substructure in NAD) is 1.6 Å. (C) Closeup view highlighting the spermidine binding site. GC-7 is shown as the white stick. Lys329 in **11g**-bound form is pointed away from spermidine binding site, and Lys287 in the α-helix in GC-7 bound form dramatically moves and overlaps the spermidine binding site instead.

The **11g** binding to the allosteric pocket unfolds the α-helix to its original state, and induces a steric clash with NAD by flipping Gly282, and spermidine by the movements

of Lys287 simultaneously. Although further investigations are required, our data implied that DHPS protein exists in the equilibrium of at least two confirmations (α-helix folded vs unfolded), which would regulate enzymatic activities (Figure 6). As the α-helix unfolded conformation does not accommodate a cofactor NAD molecule, it is inactive for enzymatic reaction. Binding of **11g** to the DHPS protein plausibly shifts the equilibrium to the inactive conformation allosterically. This may explain why **11g** binds to the allosteric pocket and exhibits DHPS inhibitory activity in a spermidine/NAD competitive manner. Although additional mechanistic studies under physiological conditions in cellular settings will be necessary, our allosteric modulator **11g** sheds light on the molecular mechanism of DHPS function.

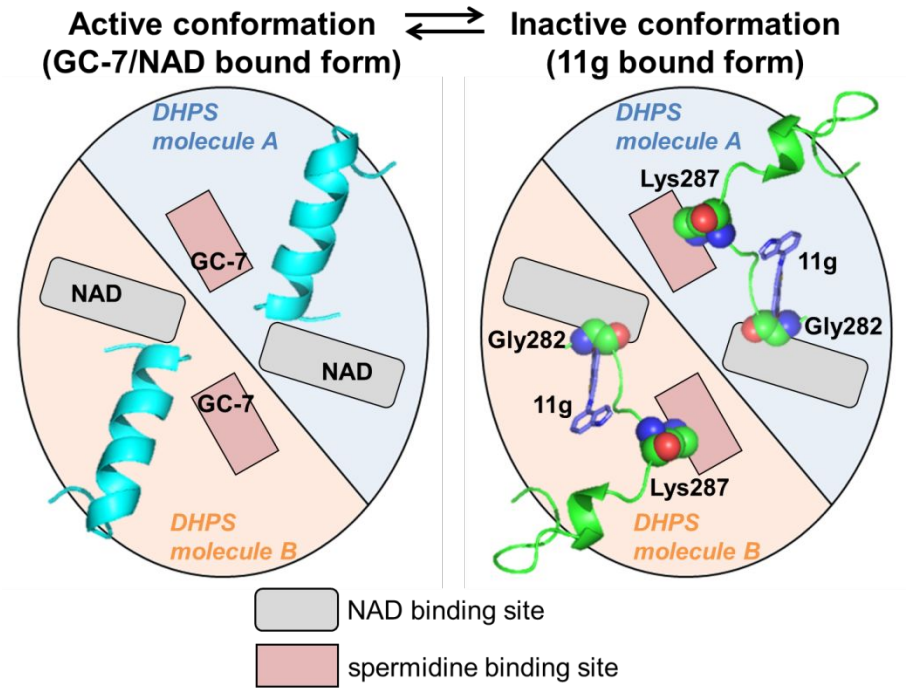

Figure 6. Schematic diagram of conformational change by **11g** binding in one dimer of a tetramer of DHPS. The binding sites of spermidines are shown in the rectangle and NAD as the rectangle with rounded corners. The **11g** binding causes the unfolding of the α-helix in the original state, and introduces steric clash with NAD by flips of Gly282 and spermidine by the movements of Lys287.

CHEMISTRY

Scheme 1 and Scheme 2 depict the synthesis of 4-*tert*-butylphenyl derivatives. Indole derivatives **5a–b** and **7** were synthesized as illustrated in Scheme 1. The treatment of commercially available amine **3** with 4-*tert*-butylbenzenesulfonyl chloride or 4-*tert*-butylphenyl isocyanate followed by the removal of the Boc group under acidic conditions generated **5a** and **5b**, respectively. Compound **7** was prepared by the condensation of carboxylic acid **6** with 4-*tert*-butylaniline. 4-*tert*-Butylbenzamide derivatives **9a–d** with a fused ring were synthesized by the treatment of 4-*tert*-butylbenzoyl chloride with the corresponding amines **8a–d**.

Scheme 1. Synthesis of Indole Derivatives **5a, b** and **7**[a]

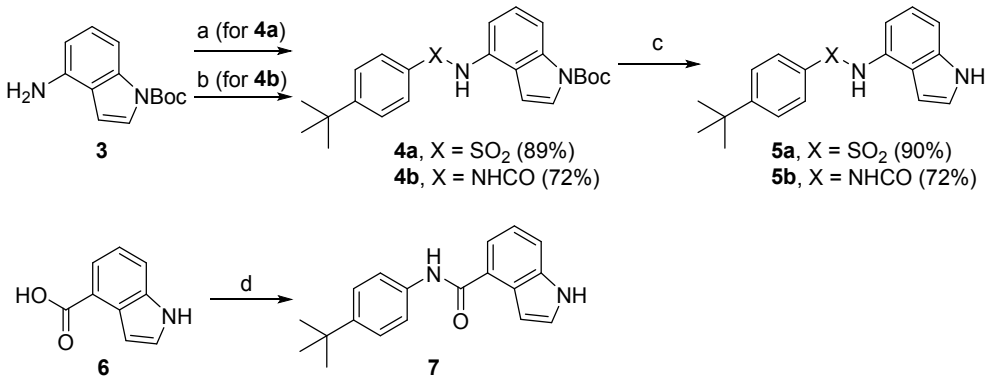

[a] Reagents and conditions: (a) 4-*tert*-butylbenzenesulfonyl chloride, pyridine, 0 °C; (b) 4-*tert*-butylphenyl isocyanate, THF; (c) TFA, MeCN; (d) 4-*tert*-butylaniline, EDC-HCl, HOBt-H_2O, Et_3N, DMF, 64%.

Scheme 2. Synthesis of Compounds **9a–d** [a]

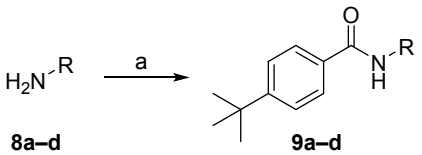

compd	R	yield (%)
8a, 9a	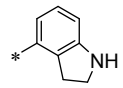	2
8b, 9b	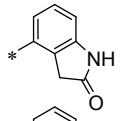	53
8c, 9c	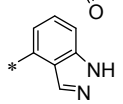	28
8d, 9d		71

[a] Reagents and conditions: (a) 4-*tert*-butylbenzoyl chloride, pyridine, 0 ºC.

The syntheses of compounds **11a–i** and **12a–c** were performed as shown in Scheme 3. Amidation of **3** with benzoyl chloride produced compound **11a**, and amide derivatives **11b–i** were similarly synthesized using acid chlorides prepared from carboxylic acids **10b–i** and oxalyl chloride. **10d** was synthesized from 6-bromobenzothiophene **13** via a nickel-catalyzed Kumada coupling reaction[26] and subsequent hydrolysis of the ethyl ester. Reductive debromination of 6-bromobezothiopene derivative **11g** produced compound **12a**. The 6-carboxamide derivative **12b** was prepared by hydrolysis of

cyanide **11e**. Copper-catalyzed iodination of **11g** in the presence of NaI and *N*,*N*-dimethylethylenediamine at 120 °C in NMP afforded iodide derivative **12c**.

Scheme 3. Synthesis of Compounds **11a–i** and **12a–c**[a]

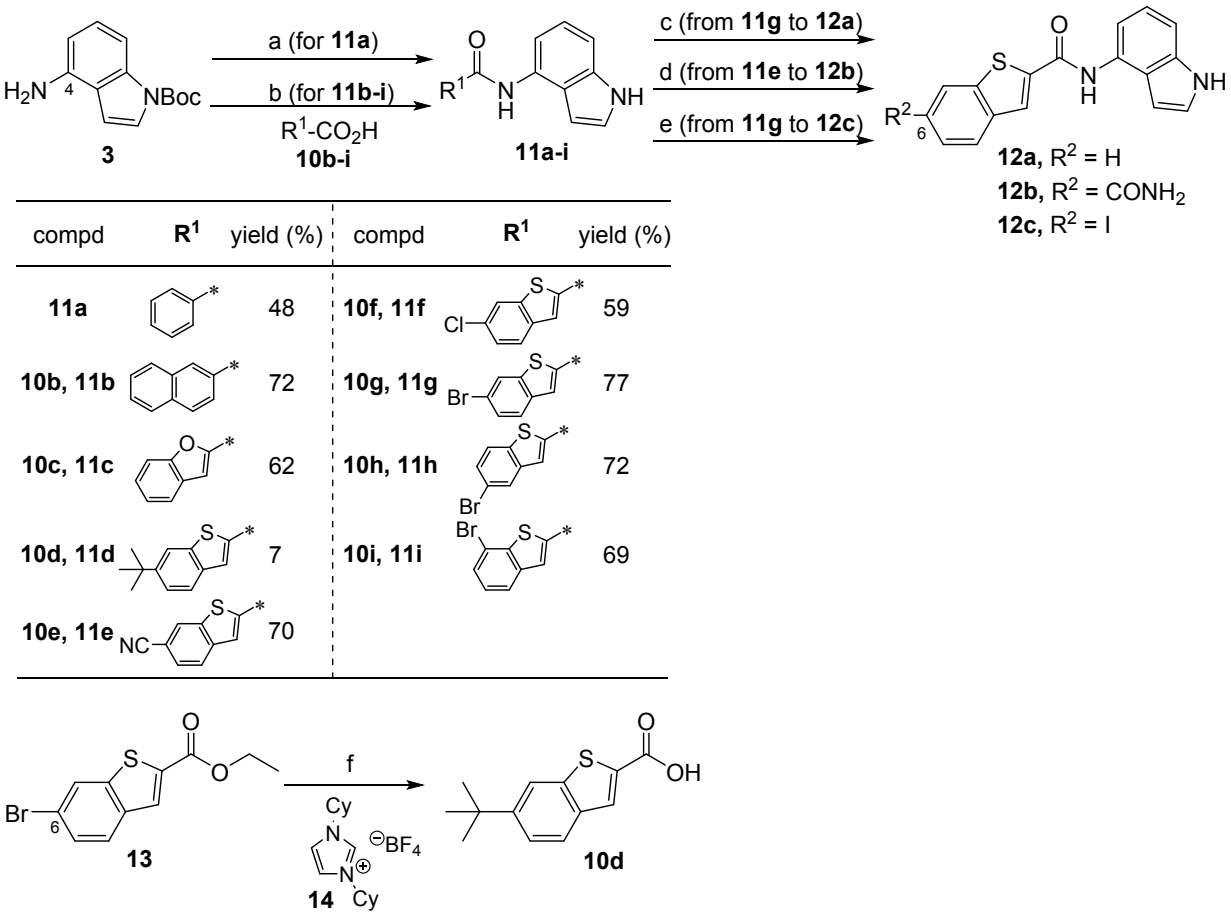

compd	R^1	yield (%)	compd	R^1	yield (%)
11a		48	**10f, 11f**		59
10b, 11b		72	**10g, 11g**		77
10c, 11c		62	**10h, 11h**		72
10d, 11d		7	**10i, 11i**		69
10e, 11e		70			

[a] Reagents and conditions: (a) (i) benzoyl chloride, THF; (ii) TFA, toluene; (b) (i) **10b–i**, oxalyl chloride, DMF, THF; (ii) TFA, toluene; (c) 10% Pd/C, H_2, EtOH, THF, 68%; (d) K_2CO_3, 35% H_2O_2, DMSO, 94%; (e) CuI, NaI, *N*,*N*-dimethylethylenediamine, NMP, 120

°C, 18%; (f) (i) **14**, *tert*-butyl magnesium chloride, nickel(II) chloride hexahydrate, THF, −15 °C; (ii) 2 M NaOH, EtOH, 2%.

CONCLUSIONS

We discovered a novel allosteric DHPS inhibitor **11g** with potent inhibitory activity against DHPS (IC_{50} = 0.062 μM). The co-crystal structure of **11g** with DHPS clarified its binding mode, which elucidated our SAR studies. The newly found structure of DHPS bearing **11g** suggested the existence of the inactive conformation of DHPS where cofactor NAD is not accommodated. **11g** is a unique molecule that binds to the allosteric site and inhibits DHPS in a spermidine/NAD competitive manner. Although the therapeutic potential of this molecule and analogs need to be further evaluated, these findings provide a new foundation for a structure-based design of allosteric inhibitors targeting DHPS, and provides a better understanding of the molecular mechanisms of the hypusine synthesis pathway.

EXPERIMENTAL SECTION

General Chemistry Information. Proton nuclear magnetic resonance (^{1}H NMR) spectra were measured with Bruker DPX-300 (300 MHz), AVANCE II-300 (300 MHz) spectrometers. Chemical shifts are given in parts per million (ppm) with tetramethylsilane as an internal standard, and coupling constants (*J* values) are given in Hertz (Hz). Splitting patterns and apparent multiplicities are designated as s (singlet), d (doublet), dd (doublet doublet), t (triplet), q (quartet), m (multiplet), and br s (broad singlet). Elemental analyses and high-resolution mass spectrometry (HRMS) were carried out by Sumika Chemical Analysis Service or Toray Research Center and were within 0.4% of the theoretical values. Analytical thin layer chromatography (TLC) was performed on silica gel 60 F_{254} plates (Merck) or NH TLC plate (Fuji Silysia Chemical Ltd.). Column chromatography was carried out using silica gel (70–230 mesh, Merck), basic silica gel (100–200 mesh, Fuji Silysia Chemical, Ltd.) or Purif-Pack (SI ϕ 60 μM or NH ϕ 60 μM, Fuji Silysia Chemical, Ltd.). Preparative HPLC was performed on a Waters 2525 separations module (L-column2 ODS (20 x150 mm I.D., CERI, Japan);

0.1% TFA in distilled water–acetonitrile gradient; MS spectra were recorded using a Waters ZQ2000 with electrospray ionization. The purities of all tested compounds were determined to be ≥95% by Shimadzu UFLC/MS (Prominence UFLC high pressure gradient system/LCMS-2020) operating in electron spray ionization mode (ESI+). The column used was an L-column 2 ODS (3.0 x 50 mm I.D., 3 μm, CERI, Japan) with a temperature of 40 °C and a flow rate of 1.2 or 1.5 mL/min. Mobile phase A was 0.05% TFA in ultrapure water. Mobile phase B was 0.05% TFA in acetonitrile which was increased linearly from 5% to 90% over 2 minutes, 90% over the next 1.5 minutes, after which the column was equilibrated to 5% for 0.5 minutes. All commercially available solvents and reagents were used without further purification, unless otherwise stated. Yields were not optimized.

***tert*-Butyl 4-(4-(*tert*-butyl)phenylsulfonamido)-1*H*-indole-1-carboxylate (4a).** To a solution of **3** (317 mg, 1.36 mmol) in pyridine (5.0 mL) was added 4-*tert*-butylbenzenesulfonyl chloride (333 mg, 1.43 mmol) at 0 °C. The mixture was stirred at 0 °C for 1 h. The mixture was poured into saturated aqueous NH_4Cl and

extracted with EtOAc. The organic layer was separated, washed with brine, dried over Na_2SO_4, and concentrated in vacuo. The residue was purified by column chromatography (silica gel, eluted with 3–20% EtOAc in *n*-hexane) to give **4a** (520 mg, 89%) as a white powder. MS (ESI+): 429.1 $[M + H]^+$. ^1H NMR (DMSO-d_6, 300 MHz): δ 1.23 (9H, s), 1.59 (9H, s), 6.82 (1H, dd, J = 3.8, 0.6 Hz), 7.06-7.13 (1H, m), 7.15–7.24 (1H, m), 7.47–7.56 (3H, m), 7.61–7.68 (2H, m), 7.78 (1H, d, J = 8.1 Hz), 10.22 (1H, s).

***tert*-Butyl 4-(3-(4-(*tert*-butyl)phenyl)ureido)-1*H*-indole-1-carboxylate (4b).** To a solution of **3** (329 mg, 1.42 mmol) in THF (4.0 mL) was added 4-*tert*-butylphenyl isocyanate (0.302 mL, 1.70 mmol) at room temperature. The mixture was stirred at room temperature for 5 h. The mixture was poured into water and extracted with EtOAc. The organic layer was separated, washed with brine, dried over Na_2SO_4, and concentrated in vacuo. The residue was purified by column chromatography (silica gel, eluted with 3–20% EtOAc in *n*-hexane) to give **4b** (415 mg, 72%) as a white powder. MS (ESI+): 408.0 $[M + H]^+$. ^1H NMR (DMSO-d_6, 300 MHz): δ 1.27 (9H, s), 1.63 (9H, s), 6.83

(1H, d, J = 3.4 Hz), 7.24 (1H, t, J = 8.2 Hz), 7.28–7.35 (2H, m), 7.36–7.44 (2H, m), 7.63–7.74 (2H, m), 7.87 (1H, d, J = 7.4 Hz), 8.65 (1H, s), 8.78 (1H, s).

4-(*tert*-Butyl)-*N*-(1*H*-indol-4-yl)benzenesulfonamide (5a). To a solution of **4a** (230 mg, 0.54 mmol) in MeCN (2.0 mL) was added TFA (2.0 mL, 26.0 mmol) at room temperature. The mixture was stirred at room temperature overnight. The mixture was neutralized with saturated aqueous $NaHCO_3$ and saturated aqueous NH_4Cl at 0 °C and extracted with EtOAc. The organic layer was separated, washed with brine, dried over Na_2SO_4, and concentrated in vacuo. The residue was filtered through silica gel pad using EtOAc. The filtrate was concentrated in vacuo, and the resulting solid was collected by filtration to give **5a** (159 mg, 90%) as a white solid. MS (ESI+): 328.9 $[M + H]^+$. ^1H NMR (DMSO-d_6, 300 MHz): δ 1.23 (9H, s), 6.61 (1H, t, J = 2.2 Hz), 6.85–6.96 (2H, m), 7.07–7.12 (1H, m), 7.16–7.22 (1H, m), 7.46–7.55 (2H, m), 7.66–7.75 (2H, m), 10.01 (1H, s), 11.07 (1H, brs). Anal. Calcd for $C_{18}H_{20}N_2O_2S$: C, 65.83; H, 6.14; N, 8.53. Found: C, 65.65; H, 6.20; N, 8.29.

1-(4-(*tert*-Butyl)phenyl)-3-(1*H*-indol-4-yl)urea (5b). Compound **5b** was synthesized from **4b** by the procedure described for **5a**. Yield 72%, a white solid. MS (ESI+): 308.0 $[M + H]^+$. ^1H NMR (DMSO-d_6, 300 MHz): δ 1.27 (9H, s), 6.55 (1H, t, J = 2.2 Hz), 6.95–7.07 (2H, m), 7.27–7.34 (3H, m), 7.37–7.44 (2H, m), 7.66 (1H, dd, J = 7.2, 1.2 Hz), 8.43 (1H, s), 8.82 (1H, s), 11.12 (1H, brs). Anal. Calcd for $C_{19}H_{21}N_3O \cdot 0.20H_2O$: C, 73.38; H, 6.94; N, 13.51. Found: C, 73.64; H, 7.04; N, 13.27.

***N*-(4-(*tert*-Butyl)phenyl)-1*H*-indole-4-carboxamide (7).** EDC-HCl (860 mg, 4.49 mmol), HOBt-H_2O (687 mg, 4.49 mmol) and Et_3N (1.25 mL, 8.97 mmol) were added to a solution of **6** (482 mg, 2.99 mmol) and 4-*tert*-butylaniline (0.572 mL, 3.59 mmol) in DMF (4.0 mL) at 0 °C. The mixture was stirred at room temperature overnight. The reaction mixture was diluted with water and extracted with EtOAc. The organic layer was washed with brine, dried over Na_2SO_4, and concentrated in vacuo. The residue was purified by column chromatography (NH silica gel, eluted with 35–75% EtOAc in *n*-hexane) to give **7** (560 mg, 64%) as a white solid. MS (ESI+): 239.1 $[M + H]^+$. ^1H NMR ($CDCl_3$, 300 MHz): δ 1.30–1.39 (9H, m), 6.93–7.07 (1H, m), 7.23–7.33 (1H, m), 7.33–

7.48 (3H, m), 7.48–7.69 (4H, m), 7.91 (1H, brs), 8.48 (1H, brs). Anal. Calcd for $C_{19}H_{20}N_2O \cdot 0.50H_2O$: C, 75.72; H, 7.02; N, 9.29. Found: C, 75.73; H, 6.83; N, 9.41.

4-(*tert*-Butyl)-*N*-(indolin-4-yl)benzamide (9a). To a solution of **8a** (91 mg, 0.68 mmol) in pyridine (3.0 mL) was added 4-*tert*-butylbenzoyl chloride (0.132 mL, 0.68 mmol) at 0 °C. The mixture was stirred at 0 °C for 30 min. The mixture was poured into water and extracted with EtOAc. The organic layer was separated, washed with brine, dried over Na_2SO_4, and concentrated in vacuo. The residue was purified by column chromatography (silica gel, eluted with 3–50% EtOAc in *n*-hexane) to give **9a** (3.9 mg, 2%) as a white solid. MS (ESI+): 295.0 $[M + H]^+$. ^{1}H NMR (DMSO-d_6, 300 MHz): δ 1.32 (9H, s), 2.86 (2H, t, J = 8.5 Hz), 3.35–3.46 (2H, m), 5.51 (1H, s), 6.35 (1H, d, J = 7.3 Hz), 6.64 (1H, d, J = 7.4 Hz), 6.86–6.94 (1H, m), 7.52 (2H, d, J = 8.6 Hz), 7.87 (2H, d, J = 8.6 Hz), 9.71 (1H, s). Anal. Calcd for $C_{19}H_{22}N_2O \cdot 0.20H_2O$: C, 76.58; H, 7.58; N, 9.40. Found: C, 76.69; H, 7.61; N, 9.29.

4-(*tert*-Butyl)-*N*-(2-oxoindolin-4-yl)benzamide (9b). Compound **9b** was synthesized from **8b** by the procedure described for **9a**. Yield 53%, a white solid. MS (ESI+): 309.0

[M + H]$^+$. ^{1}H NMR (DMSO-d_6, 300 MHz): δ 1.32 (9H, s), 3.47 (2H, s), 6.67 (1H, dd, J = 7.0, 1.5 Hz), 7.09–7.24 (2H, m), 7.50–7.60 (2H, m), 7.83–7.93 (2H, m), 9.95 (1H, s), 10.42 (1H, s). Anal. Calcd for $C_{19}H_{20}N_2O_2 \cdot 0.30H_2O$: C, 72.73; H, 6.62; N, 8.93. Found: C, 72.76; H, 6.59; N, 8.77.

4-(*tert*-Butyl)-*N*-(1*H*-indazol-4-yl)benzamide (9c). Compound **9c** was synthesized from **8c** by the procedure described for **9a**. Yield 28%, a white solid. MS (ESI+): 294.2 [M + H]$^+$. ^{1}H NMR (DMSO-d_6, 300 MHz): δ 1.34 (9H, s), 7.24–7.43 (2H, m), 7.44–7.70 (3H, m), 7.87–8.03 (2H, m), 8.22 (1H, s), 10.33 (1H, s), 13.05 (1H, brs). Anal. Calcd for $C_{18}H_{19}N_3O$: C, 73.70; H, 6.53; N, 14.32. Found: C, 73.35; H, 6.59; N, 14.21.

4-(*tert*-Butyl)-*N*-(1*H*-indazol-7-yl)benzamide (9d). Compound **9d** was synthesized from **8d** by the procedure described for **9a**. Yield 71%, a white solid. MS (ESI+): 294.2 [M + H]$^+$. ^{1}H NMR (DMSO-d_6, 300 MHz): δ 1.34 (9H, s), 7.12 (1H, t, J = 7.7 Hz), 7.54–7.69 (4H, m), 7.98 (2H, d, J = 8.3 Hz), 8.10 (1H, d, J = 1.1 Hz), 10.19 (1H, s), 12.84 (1H, s). Anal. Calcd for $C_{18}H_{19}N_3O$: C, 73.70; H, 6.53; N, 14.32. Found: C, 73.57; H, 6.56; N, 14.34.

6-*tert*-Butyl-1-benzothiophene-2-carboxylic acid (10d). To a solution of **13** (3.10 g, 10.9 mmol) in THF (30 mL) were added **14** (0.348 g, 1.09 mmol), nickel(II) chloride hexahydrate (0.258 g, 1.09 mmol) and a 1.7M solution of *tert*-butylmagnesium chloride in THF (12.5 mL, 21.3 mmol) at -15 °C. The mixture was stirred at –15 °C under Ar for 4 h. The mixture was poured into saturated aqueous NH_4Cl at 0 °C and extracted with EtOAc. The organic layer was separated, washed with brine, dried over Na_2SO_4, and concentrated in vacuo. The residue was purified by column chromatography (silica gel, eluted with 0–3% EtOAc in *n*-hexane) to give a crude product. This product was subjected to the next reaction without further purification. To a solution of the product in EtOH (20 mL) was added 2M NaOH (10 mL, 20.0 mmol) at room temperature. The mixture was stirred at room temperature for 1 h. The mixture was concentrated in vacuo, and the resulting solid was dissolved in water. The solution was acidified with 1M HCl at 0 °C and extracted with EtOAc. The organic layer was separated, washed with brine, dried over Na_2SO_4, and concentrated in vacuo. The residue was purified by column chromatography (silica gel, eluted with 10–100% EtOAc in *n*-hexane) to give

10d (0.054 g, 2%) as a white solid. ^{1}H NMR (DMSO-d_6, 300 MHz): δ 1.35 (9H, s), 7.50–7.57 (1H, m), 7.90 (1H, d, J = 8.5 Hz), 7.97–8.03 (2H, m), 12.88 (1H, brs).

***N*-(1*H*-Indol-4-yl)benzamide (11a).** To a solution of **3** (80.0 mg, 0.34 mmol) in pyridine (2.0 mL) was added benzoyl chloride (0.048 mL, 0.41 mmol) at room temperature. The mixture was stirred at room temperature for 1 h. The mixture was poured into water and extracted with EtOAc. The organic layer was separated, washed with brine, and dried over Na_2SO_4. The mixture was filtered through silica gel pad using EtOAc and the filtrate was concentrated in vacuo. This product was subjected to the next reaction without further purification. To a solution of the crude product in toluene (5.0 mL) was added TFA (2.0 mL, 26.0 mmol) at room temperature. The mixture was stirred at room temperature for 1 h, and then concentrated in vacuo. The residue was neutralized with saturated aqueous $NaHCO_3$ and extracted with EtOAc. The organic layer was separated, washed with brine, dried over Na_2SO_4, and concentrated in vacuo. The residue was purified by column chromatography (silica gel, eluted with 3–30% EtOAc in *n*-hexane) to give **11a** (34.9 mg, 48%) as a white solid. MS (ESI+): 236.9 [M +

H]$^+$. ^{1}H NMR (DMSO-d_6, 300 MHz): δ 6.56–6.62 (1H, m), 7.01–7.12 (1H, m), 7.24 (1H, d, J = 8.0 Hz), 7.28–7.32 (1H, m), 7.38 (1H, d, J = 7.5 Hz), 7.49–7.63 (3H, m), 7.96–8.05 (2H, m), 10.06 (1H, s), 11.12 (1H, brs). Anal. Calcd for $C_{15}H_{12}N_2O$: C, 76.25; H, 5.12; N, 11.86. Found: C, 75.98; H, 5.05; N, 11.75.

***N*-(1*H*-Indol-4-yl)-2-naphthamide (11b).** To a solution of **10b** (77 mg, 0.45 mmol) in THF (3.0 mL) were added $(COCl)_2$ (0.039 mL, 0.45 mmol) and DMF (2.67 μL, 0.03 mmol) at room temperature. The mixture was stirred at room temperature for 30 min. The mixture was concentrated in vacuo. The mixture was added to a solution of **3** (80.0 mg, 0.34 mmol) in pyridine (3.0 mL) at room temperature and stirred at room temperature for 1 h. The mixture was poured into water and extracted with EtOAc. The organic layer was separated, washed with brine, and dried over Na_2SO_4. The mixture was filtered through silica gel pad using EtOAc and the filtrate was concentrated in vacuo. This product was subjected to the next reaction without further purification. To a solution of the crude product in toluene (5.0 mL) was added TFA (2.0 mL, 26.0 mmol) at room temperature. The mixture was stirred at room temperature for 1 h, and then

concentrated in vacuo. The mixture was neutralized with saturated aqueous $NaHCO_3$ and extracted with EtOAc. The organic layer was separated, washed with brine, and dried over Na_2SO_4. The mixture was filtered through silica gel pad using EtOAc and the filtrate was concentrated in vacuo. The resulting solid was collected by filtration to give **11b** (61.8 mg, 72%) as a white solid. MS (ESI+): 286.9 $[M + H]^+$. ^1H NMR (DMSO-d_6, 300 MHz): δ 6.65 (1H, t, J = 2.1 Hz), 7.05–7.14 (1H, m), 7.26 (1H, d, J = 8.1 Hz), 7.29–7.35 (1H, m), 7.43 (1H, d, J = 7.4 Hz), 7.58–7.69 (2H, m), 7.98–8.15 (4H, m), 8.64 (1H, s), 10.23 (1H, s), 11.15 (1H, brs). Anal. Calcd for $C_{19}H_{14}N_2O \cdot 0.10H_2O$: C, 79.20; H, 4.97; N, 9.72. Found: C, 79.15; H, 4.88; N, 9.59.

***N*-(1*H*-Indol-4-yl)-1-benzofuran-2-carboxamide (11c).** Compound **11c** was synthesized from **3** and **10c** by the procedure described for **11b**. Yield 62%, a white solid. MS (ESI+): 276.9 $[M + H]^+$. ^1H NMR (DMSO-d_6, 300 MHz): δ 6.54–6.61 (1H, m), 7.05–7.13 (1H, m), 7.28 (1H, d, J = 8.1 Hz), 7.31–7.42 (3H, m), 7.47–7.56 (1H, m), 7.74 (1H, dd, J = 8.3, 0.8 Hz), 7.79–7.87 (2H, m), 10.25 (1H, s), 11.18 (1H, brs). Anal. Calcd for $C_{17}H_{12}N_2O_2$: C, 73.90; H, 4.38; N, 10.14. Found: C, 74.02; H, 4.46; N, 9.91.

6-*tert*-Butyl-*N*-(1*H*-indol-4-yl)-1-benzothiophene-2-carboxamide (11d). Compound **11d** was synthesized from **3** and **10d** by the procedure described for **11b**. Yield 7%, a white solid. MS (ESI+): 349.0 $[M + H]^+$. ^1H NMR (DMSO-d_6, 300 MHz): δ 1.37 (9H, s), 6.61 (1H, brs), 7.04–7.13 (1H, m), 7.27 (1H, d, J = 8.0 Hz), 7.30–7.39 (2H, m), 7.56 (1H, dd, J = 8.5, 1.7 Hz), 7.91 (1H, d, J = 8.5 Hz), 8.03 (1H, s), 8.38 (1H, s), 10.29 (1H, s), 11.17 (1H, brs). HRMS-ESI (*m/z*): [M + Na] calcd for $C_{21}H_{20}N_2NaOS$, 371.1194; found. 371.1197.

6-Cyano-*N*-(1*H*-indol-4-yl)-1-benzothiophene-2-carboxamide (11e). Compound **11e** was synthesized from **3** and **10e** by the procedure described for **11b**. Yield 70%, a white solid. MS (ESI+): 317.9 $[M + H]^+$. ^1H NMR (DMSO-d_6, 300 MHz): δ 6.61 (1H, brs), 7.05–7.17 (1H, m), 7.24–7.42 (3H, m), 7.85 (1H, d, J = 8.3 Hz), 8.20 (1H, d, J = 8.2 Hz), 8.54 (1H, s), 8.72 (1H, s), 10.54 (1H, s), 11.20 (1H, brs). Anal. Calcd for $C_{18}H_{11}N_3O_2 \cdot 0.25H_2O$: C, 67.17; H, 3.60; N, 13.05. Found: C, 67.39; H, 3.67; N, 12.68.

6-Chloro-*N*-(1*H*-indol-4-yl)-1-benzothiophene-2-carboxamide (11f). Compound **11f** was synthesized from **3** and **10f** by the procedure described for **11b**. Yield 59%, a

yellow solid. MS (ESI+): 326.8 $[M + H]^+$. ^1H NMR (DMSO-d_6, 300 MHz): δ 6.61 (1H, t, J = 2.2 Hz), 7.05–7.13 (1H, m), 7.28 (1H, d, J = 8.1 Hz), 7.31–7.38 (2H, m), 7.51 (1H, dd, J = 8.6, 2.0 Hz), 8.02 (1H, d, J = 8.6 Hz), 8.25 (1H, d, J = 1.9 Hz), 8.44 (1H, s), 10.40 (1H, s), 11.18 (1H, brs). Anal. Calcd for $C_{17}H_{11}N_2OSCl$: C, 62.48; H, 3.39; N, 8.57. Found: C,62.24; H, 3.51; N, 8.37.

6-Bromo-*N*-(1*H*-indol-4-yl)-1-benzothiophene-2-carboxamide (11g). Compound **11g** was synthesized from **3** and **10g** by the procedure described for **11b**. Yield 77%, a yellow solid. MS (ESI+): 370.8 $[M + H]^+$. ^1H NMR (DMSO-d_6, 300 MHz): δ 6.61 (1H, brs), 7.04–7.15 (1H, m), 7.24–7.38 (3H, m), 7.63 (1H, dd, J = 8.6, 1.8 Hz), 7.96 (1H, d, J = 8.5 Hz), 8.35–8.47 (2H, m), 10.41 (1H, s), 11.18 (1H, brs). Anal. Calcd for $C_{17}H_{11}N_2OSBr$: C, 55.00; H, 2.99; N, 7.55. Found: C, 55.03; H, 2.92; N, 7.44.

5-Bromo-*N*-(1*H*-indol-4-yl)-1-benzothiophene-2-carboxamide (11h). Compound **11h** was synthesized from **3** and **10h** by the procedure described for **11b**. Yield 72%, a white solid. MS (ESI+): 370.8 $[M + H]^+$. ^1H NMR (DMSO-d_6, 300 MHz): δ 6.55–6.64 (1H, m), 7.03–7.15 (1H, m), 7.23–7.40 (3H, m), 7.63 (1H, dd, J = 8.6, 2.0 Hz), 8.05 (1H, d, J

= 8.6 Hz), 8.26 (1H, d, *J* = 1.9 Hz), 8.39 (1H, s), 10.47 (1H, s), 11.18 (1H, brs). Anal. Calcd for $C_{17}H_{11}N_2OSBr$: C, 55.00; H, 2.99; N, 7.55. Found: C, 55.01; H, 3.12; N, 7.44.

7-Bromo-*N*-(1*H*-indol-4-yl)-1-benzothiophene-2-carboxamide (11i). Compound **11i** was synthesized from **3** and **10i** by the procedure described for **11b**. Yield 69%, a white solid. MS (ESI+): 370.8 $[M + H]^+$. ^1H NMR (DMSO-d_6, 300 MHz): δ 6.58–6.65 (1H, m), 7.06–7.14 (1H, m), 7.29 (1H, d, *J* = 8.1 Hz), 7.32–7.38 (2H, m), 7.45 (1H, t, *J* = 7.8 Hz), 7.76 (1H, dd, *J* = 7.6, 0.8 Hz), 8.06 (1H, dd, *J* = 8.0, 0.7 Hz), 8.60 (1H, s), 10.46 (1H, s), 11.19 (1H, brs). Anal. Calcd for $C_{17}H_{11}N_2OSBr$: C, 55.00; H, 2.99; N, 7.55. Found: C, 54.95; H, 3.04; N, 7.37.

***N*-(1*H*-Indol-4-yl)-1-benzothiophene-2-carboxamide (12a).** A mixture of **11g** (50.0 mg, 0.13 mmol) and 10% Pd-C (160 mg, 0.13 mmol) in EtOH (1.0 mL) and THF (1.0 mL) was hydrogenated under balloon pressure at room temperature for 3 h. The catalyst was removed by filtration and the filtrate was concentrated in vacuo. The residue was purified by column chromatography (silica gel, eluted with 3–30% EtOAc in *n*-hexane) to give **12a** (26.6 mg, 68 %) as a pale yellow solid. MS (ESI+): 292.9 $[M + H]^+$. ^1H NMR

(DMSO-d_6, 300 MHz): δ 6.59–6.64 (1H, m), 7.05–7.13 (1H, m), 7.27 (1H, d, J = 8.1 Hz), 7.31–7.38 (2H, m), 7.44–7.54 (2H, m), 7.96–8.10 (2H, m), 8.45 (1H, s), 10.35 (1H, s), 11.18 (1H, brs). Anal. Calcd for $C_{17}H_{12}N_2OS \cdot 0.30H_2O$: C, 68.57; H, 4.27; N, 9.41. Found: C, 68.61; H, 4.16; N, 9.30.

***N*²-(1*H*-indol-4-yl)-1-benzothiophene-2,6-dicarboxamide (12b).** To a solution of **11e** (30.0 mg, 0.09 mmol) in DMSO (1.0 mL) were added K_2CO_3 (15.7 mg, 0.11 mmol) and 35% H_2O_2 (0.025 mL, 0.28 mmol) at 0 °C. The mixture was stirred at room temperature for 3 h. The mixture was poured into water and extracted with EtOAc. The organic layer was separated, washed with brine, dried over Na_2SO_4, and concentrated in vacuo. The resulting solid was collected by filtration to give **12b** (29.8 mg, 94 %) as a yellow solid. MS (ESI+): 335.9 $[M + H]^+$. ^{1}H NMR (DMSO-d_6, 300 MHz): δ 6.62 (1H, brs), 7.05–7.15 (1H, m), 7.24–7.39 (3H, m), 7.49 (1H, brs), 7.91–7.99 (1H, m), 8.02–8.18 (2H, m), 8.49 (1H, s), 8.56 (1H, s), 10.44 (1H, s), 11.19 (1H, brs). HRMS-ESI (*m/z*): [M + Na] calcd for $C_{18}H_{13}N_3NaO_2S$, 358.0626; found. 358.0643.

***N*-(1*H*-indol-4-yl)-6-iodo-1-benzothiophene-2-carboxamide (12c).** To a solution of **11g** (100 mg, 0.27 mmol) in NMP (2.0 mL) were added NaI (202 mg, 1.35 mmol), *N*,*N*-dimethyl-1,2-ethanediamine (0.029 mL, 0.27 mmol) and copper(I) iodide (25.6 mg, 0.13 mmol) at room temperature. The mixture was stirred at 120 °C under N_2 overnight. The mixture was poured into water and extracted with EtOAc. The organic layer was separated, washed with brine, dried over Na_2SO_4, and concentrated in vacuo. The residue was purified by column chromatography (silica gel, eluted with 3–50% EtOAc in *n*-hexane) to give a crude product. The product was purified by preparative HPLC (L-Column 2 ODS, eluted with H_2O in acetonitrile containing 0.1% TFA) to give **12c** (20.7 mg, 18%) as a pale yellow solid. MS (ESI+): 418.8 $[M + H]^+$. ^1H NMR (DMSO-d_6, 300 MHz): δ 6.57–6.63 (1H, m), 7.05–7.13 (1H, m), 7.27 (1H, d, J = 8.1 Hz), 7.31–7.37 (2H, m), 7.73–7.84 (2H, m), 8.41 (1H, s), 8.53 (1H, s), 10.40 (1H, s), 11.18 (1H, brs). Anal. Calcd for $C_{17}H_{11}N_2OSI$: C, 48.82; H, 2.65; N, 6.70. Found: C, 48.66; H, 2.61; N, 6.68.

In vitro enzyme assay. The reaction mixture contained 1 μM eIF5A, 2 μM [^{3}H]-spermidine trihydrochloride (38.5 Ci/mmol), 14 μM nicotinamide adenine dinucleotide (NAD^+)(K_m), 1 mM DTT, various concentrations of the inhibitor, and 24 nM DHPS in 50 mM Tris-HCl buffer, pH 8.0. For analysis of higher concentrations of NAD^+, the enzyme reactions were performed in buffer containing 1 μM eIF5A, 2 μM [^{3}H]-spermidine trihydrochloride, and 250 μM NAD^+ (×18 K_m). After a 120-min incubation at room temperature, incorporation of radio-labeled aminobutylidene was terminated by the addition of 20 μL of 300 μM GC-7; 25 μL of the stopped reaction was transferred to a streptavidin (SA) plate (NeutrAvidin Coated Plates, Thermo Scientific Cat. No. 15512), and incubated for 90–120 min at room temperature to allow complete binding of all proteins to the plates. Plates were washed three times with PBS, and 50 μL of scintillation cocktail was added (OptiPhase“SuperMix” from PerkinElmer). The plate was measured with TOP count (PerkinElmer).

Protein Expression and Purification. The cDNA encoding the entire open reading frame of the human DHPS (GenBank accession number: NM_001930) gene was

amplified by PCR and engineered to contain an N-terminal hexahistidine affinity tag and a recognition site for the TEV protease to facilitate purification. The product was cloned into a modified pET28a+ vector and verified by DNA sequence analysis. For expression, the plasmid was transformed into BL21(DE3) *E. coli* (Life Technologies). Cells were cultured at 37 ℃ and induced with 0.5 mM IPTG when the culture reached an O.D. of 0.8. After 4 h of induction the cells were isolated by centrifugation, and the pellets were stored at -80 ℃.

The biomass obtained from a 6 L culture was lysed in 150 mL of buffer containing 25 mM TRIS (pH 7.6), 1 M NaCl, 10 mM imidazole (buffer components were routinely purchased from Sigma-Aldrich), 0.5 mM TCEP (Thermo Scientific), 20 U/ml benzonase, 0.1 mg/mL lysozyme, and EDTA-free protease inhibitors (Roche) by homogenization and sonication (Sonics Vibra-Cell). The lysate was clarified by centrifugation at 14,000 RPM for 90 min in a JA-14 fixed angle rotor (Beckman Coulter).

DHPS was isolated from the lysate using a 5 mL HisTALON superflow cartridge (Clontech) connected to an AKTAxpress FPLC system (GE Healthcare Life Sciences).

After loading, the cartridge was washed with 100 column volumes of 25 mM TRIS (pH 7.6), 1 M NaCl, 10 mM imidazole, and 0.5 mM TCEP, followed by elution in buffer supplemented with 300 mM imidazole. The eluate from the Ni-affinity column was concentrated to 10 mL and treated with TEV protease during an overnight dialysis against 1 L of buffer composed of 25 mM TRIS (pH 7.6), 0.5 mM NaCl, 10 mM imidazole, and 0.5 mM TCEP. The cleaved product was passed over a HisTALON cartridge, the flow-through was collected and concentrated using Amicon Ultra centrifugal filter units (EMD-Millipore). A final purification step was conducted using size exclusion chromatography with a HiLoad 16/600 Superdex 200 column (GE Healthcare Life Sciences) in a buffer containing 25 mM Tris (pH 7.9) and 100 mM KCl. Peak fractions were analyzed by SDS-PAGE and the fractions containing DHPS were pooled and concentrated to 11 mg/mL before aliquoting and storage at -80 ˚C. Protein concentration was estimated using a NanoDrop instrument.

Crystallography. Prior to crystallization ligands were added at a concentration of 1–3 mM. All crystallization was performed using the hanging drop vapor diffusion method.

The NAD-DHPS complex was initially crystallized using published methods[17] in a reservoir solution containing 0.1 mM Tris (pH 8.0) and 65% MPD (Hampton Research) at room temperature. To obtain the NAD/GC7-DHPS ternary complex, the NAD-DHPS crystals were soaked with reservoir solution containing 10 mM GC-7 for three days, after which the crystals were flash-frozen directly into ALS-style pucks submerged in liquid nitrogen. The DHPS-**11g** complex was obtained by co-crystallization at room temperature using a reservoir solution composed of 1.6 M sodium/potassium phosphate (pH 6.8), prepared by mixing sodium phosphate monobasic monohydrate and potassium phosphate dibasic (Hampton Research). These crystals were quickly transferred into reservoir solution supplemented with 30% sucrose for cryo-protection and immediately flash-frozen in liquid nitrogen.

Diffraction data were collected at Advanced Light Source beamlines 5.0.3 and 5.02 (NAD-GC-7 and **11g** complexes, respectively) (Lawrence Berkeley's National Laboratory, Berkeley, CA) and processed with HKL2000.[27] The structure was solved by molecular replacement with Phaser[28] using the coordinates of human DHPS (PDB

code: 1RLZ) as a search model. The graphics program COOT[29] was used for model building, and refinement was performed with REFMAC5.[30] Phaser and REFMAC5 were distributed as part of CCP4.[31] Structure validation was performed using Molprobity.[32] Refinement statistics as reported in Supplemental Table S1 and images of the omit electron density of the ligands are shown in Supplemental Figure S2 and Figure S3.

ASSOCIATED CONTENT

Supporting Information: The Supporting Information is available free of charge via the Internet at http://pubs.acs.org.

Data collection and refinement statistics of X-ray structures, closeup view highlighting the orientation of GC-7 and omit electron density Fo-Fc maps of GC-7 and **11g**

Molecular formula strings

Accession Codes: Atom coordinates and structure factors for complexes of DHPS/compound **1**, and DHPS/compound **11g** have been deposited in the Protein Data Bank with accession codes 6P4V, and 6PGR, respectively.

AUTHOR INFORMATION

Corresponding Author

*For Y. T.: phone, +81-466-32-1164; E-mail, yuta.tanaka@takeda.com.

Author Contributions

These authors contributed equally.

Notes

The authors declare no competing financial interests.

ACKNOWLEDGMENT

We would like to thank all members of the DHPS Program Team at Takeda for their contribution. We thank Bi-Ching Sang and Irena Levin for the construct encoding DHPS; and Gyorgy Snell and Weston Lane for diffraction data collection. We also thank the staff of the Berkeley Center for Structural Biology (BCSB), who operates ALS beamline 5.0.3. The BCSB is supported in part by the US National Institutes of Health, US National Institute of General Medical Sciences. The Advanced Light Source is supported by the Director, Office of Science, Office of Basic Energy Sciences of the U.S. Department of Energy under Contract No. DE-AC02-05CH11231.

ABBREVIATIONS

DHPS, deoxyhypusine synthase; eIF5A, eukaryotic translation initiation factor 5A; DOHH, deoxyhypusine hydroxylase; NAD, nicotinamide adenine dinucleotide; SAR, structure–activity relationship.

REFERENCES

1. Park, M. H.; Wolff, E. C., Hypusine, a polyamine-derived amino acid critical for eukaryotic translation. *J. Biol. Chem.* **2018**, *293*, 18710–18718.
2. Henderson, A.; Hershey, J. W. Eukaryotic translation initiation factor (eIF) 5A stimulates protein synthesis in Saccharomyces cerevisiae. *Proc. Natl. Acad. Sci.U S A.* **2011**, *108*, 6415–6419.
3. Saini, P.; Eyler, D. E.; Green, R.; Dever, T. E. Hypusine-containing protein eIF5A promotes translation elongation. *Nature* **2009**, *459*, 118–121.
4. Guan, X. Y.; Fung, J. M.; Ma, N. F.; Lau, S. H.; Tai, L. S.; Xie, D.; Zhang, Y.; Hu, L.; Wu, Q. L.; Fang, Y.; Sham, J. S. Oncogenic role of eIF-5A2 in the development of ovarian cancer. *Cancer Res.* **2004**, *64*, 4197–4200.
5. Greganova, E.; Altmann, M.; Butikofer, P. Unique modification of translation elongation factors. *FEBS J.* **2011**, *278*, 2613–2624.
6. Park, M. H.; Nishimura, K.; Zanelli, C. F.; Valentini, S. R. Functional significance of eIF5A and its hypusine modification in eukaryotes. *Amino Acids* **2010**, *38*, 491–500.

7. Tong, Y.; Park, I.; Hong, B. S.; Nedyalkova, L.; Tempel, W.; Park, H. W. Crystal structure of human eIF5A1: insight into functional similarity of human eIF5A1 and eIF5A2. *Proteins* **2009**, *75*, 1040–1045.
8. Nishimura, K.; Ohki, Y.; Fukuchi-Shimogori, T.; Sakata, K.; Saiga, K.; Beppu, T.; Shirahata, A.; Kashiwagi, K.; Igarashi, K. Inhibition of cell growth through inactivation of eukaryotic translation initiation factor 5A (eIF5A) by deoxyspergualin. *Biochem. J.* **2002,** *363*, 761–768.
9. Puleston, D. J.; Buck, M. D.; Klein Geltink, R. I.; Kyle, R. L.; Caputa, G.; O'Sullivan, D.; Cameron, A. M.; Castoldi, A.; Musa, Y.; Kabat, A. M.; Zhang, Y.; Flachsmann, L. J.; Field, C. S.; Patterson, A. E.; Scherer, S.; Alfei, F.; Baixauli, F.; Austin, S. K.; Kelly, B.; Matsushita, M.; Curtis, J. D.; Grzes, K. M.; Villa, M.; Corrado, M.; Sanin, D. E.; Qiu, J.; Pallman, N.; Paz, K.; Maccari, M. E.; Blazar, B. R.; Mittler, G.; Buescher, J. M.; Zehn, D.; Rospert, S.; Pearce, E. J.; Balabanov, S.; Pearce, E. L. Polyamines and eIF5A hypusination modulate mitochondrial respiration and macrophage activation. *Cell Metab.* **2019**, *30*, 352–363.
10. Jakus, J.; Wolff, E. C.; Park, M. H.; Folk, J. E. Features of the spermidine-binding site of deoxyhypusine synthase as derived from inhibition studies. *J. Biol. Chem.* **1993**, *268*, 13151–13519.

11. Lee, Y. B.; Park, M. H.; Folk, J. E. Diamine and triamine analogs and derivatives as inhibitors of deoxyhypusine synthase; synthesis and biological activity. *J. Med. Chem.* **1995**, *38*, 3053–3061.

12. Lee, Y. B.; Folk, J. E. Branched-chain and unsaturated 1,7-diaminoheptane derivatives as deoxyhypusine synthase inhibitors. *Bioorg. Med. Chem.* **1998**, *6*, 253–270.

13. Ziegler, P.; Chahoud, T.; Wilhelm, T.; Pallman, N.; Braig, M.; Wiehle, V.; Ziegler, S.; Schroder, M.; Meier, C.; Kolodzik, A.; Rarey, M.; Panse, J.; Hauber, J.; Balabanov, S.; Brummendorf, T. H. Evaluation of deoxyhypusine synthase inhibitors targeting BCR-ABL positive leukemias. *Invest. New Drugs.* **2012,** *30*, 2274–2283.

14. Schroeder, M.; Kolodzik, A.; Pfaff, K.; Priyadarshini, P.; Krepstakies, M.; Hauber, J.; Rarey, M.; Meier, C. In silico design, synthesis, and screening of novel deoxyhypusine synthase inhibitors targeting HIV-1 replication. *ChemMedChem* **2014**, *9*, 940–952.

15. The PyMOL Molecular Graphics System, Version 1.4.1 Schrödinger, LLC.

16. Liao, D. I.; Wolff E. C.; Park, M. H.; Davies, D. R. Crystal structure of the NAD complex of human deoxyhypusine synthase: an enzyme with a ball-and-chain mechanism for blocking the active site. *Structure* **1998**, *6*, 23–32.

17. Umland, T. C.; Wolff, E. C.; Park, M. H.; Davies, D. R. A new crystal structure of deoxyhypusine synthase reveals the configuration of the active enzyme and of an enzyme·NAD·inhibitor ternary complex. *J. Biol. Chem.* **2004**, *279*, 28697–28705.

18. Marton, L. J.; Pegg, A. E. Polyamines as targets for therapeutic intervention. *Annu. Rev. Pharmacol. Toxicol.* **1995,** *35*, 55-91.

19. Sugiyama, S.; Vassylyev, D. G.; Matsushima, M.; Kashiwagi, K.; Igarashi, K.; Morikawa, K. Crystal structure of PotD, the primary receptor of the polyamine transport system in Escherichia coli. *J. Biol. Chem.* **1996,** *271*, 9519–9525.

20. Lee, C. H.; Um, P. Y.; Park, M. H. Structure-function studies of human deoxyhypusine synthase: identification of amino acid residues critical for the binding of spermidine and NAD. *Biochem. J.* **2001**, *355*, 841–849.

21. Lee, C. H.; Park, M. H. Human deoxyhypusine synthase: interrelationship between binding of NAD and substrates. *Biochem. J.* **2000,** *352*, 851-857.

22. Joe, Y. A.; Wolff, E. C.; Lee, Y. B.; Park, M. H. Enzyme-substrate intermediate at a specific lysine residue is required for deoxyhypusine synthesis. The role of Lys329 in human deoxyhypusine synthase. *J. Biol. Chem.* **1997**, *272*, 32679–32685.

23. Nagao, Y.; Hirata, T.; Goto, S.; Sano, S.; Kakehi, A.; Iizuka, K.; Shiro, M. Intramolecular nonbonded S···O interaction recognized in (acylimino)thiadiazoline derivatives as angiotensin II receptor antagonists and related compounds. *J. Am. Chem. Soc.* **1998**, *120*, 3104–3110.

24. Auffinger, P.; Hays, F. A.; Westhof, E.; Ho, P. S. Halogen bonds in biological molecules. *Proc. Natl. Acad. Sci.* **2004**, *101*, 16789–16794.

25. Clark, T.; Hennemann, M.; Murray, J. S.; Politzer, P.; Halogen bonding: the σ-hole. *J. Mol. Model.* **2007**, *13*, 291–296.

26. Joshi-Pangu, A.; Wang, C. Y.; Biscoe, M. R. Nickel-catalyzed Kumada cross-coupling reactions of tertiary alkylmagnesium halides and aryl bromides/triflates. *J. Am. Chem. Soc.* **2011**, *133*, 8478–8481.

27. Otwinowski, Z.; Minor, W. Processing of X-ray diffraction data collected in oscillation mode. *Methods Enzymol.* **1997**, *276*, 307–326.

28. McCoy, A. J.; Grosse-Kunstleve, R. W.; Adams, P. D.; Winn, M. D.; Storoni, L. C.; Read, R. J. Phaser crystallographic software. *J. Appl. Cryst.* **2007**, *40*, 658–674.

29. Emsley, P.; Cowtan, K. Coot: model-building tools for molecular graphics. *Acta Crystallogr. D Biol. Crystallogr.* **2004**, *60*, 2126–2132.

30. Murshudov, G. N.; Vagin, A. A.; Dodson, E. J. Refinement of macromolecular structures by the maximum-likelihood method. *Acta Crystallogr. D Biol. Crystallogr.* **1997**, *53*, 240–255.

31. Collaborative computing project. The CCP4 suite: programs for protein crystallography. *Acta Crystallogr. D Biol. Crystallogr.* **1994**, *50*, 760–763.

32. Chen, V. B.; Arendall III, W. B.; Headd, J. J.; Keedy, D. A.; Immormino, R. M.; Kapral, G. J.; Murray, L. W.; Richardson, J. S.; Richardson, D. C. MolProbity: all-atom

structure validation for macromolecular crystallography. *Acta Crystallogr. D Biol. Crystallogr.* **2010**, *66*, 12–21.

Table of Contents graphic.